ELSEVIER

Nuclear Instruments and Methods in Physics Research A 476 (2002) 569–582

NUCLEAR INSTRUMENTS & METHODS IN PHYSICS RESEARCH Section A

www.elsevier.com/locate/nima

Radiation hardness of cryogenic silicon detectors

T.O. Niinikoski[a,*], M. Abreu[b], W. Bell[c], P. Berglund[d], W. de Boer[e], E. Borchi[f], K. Borer[g], M. Bruzzi[f], S. Buontempo[h], L. Casagrande[a], S. Chapuy[i], V. Cindro[j], P. Collins[a], N. D'Ambrosio[h], C. Da Viá[k], S.R.H. Devine[c], B. Dezillie[l,1], Z. Dimcovski[i], V. Eremin[m], A. Esposito[n], V. Granata[1,k], E. Grigoriev[i], S. Grohmann[a], F. Hauler[c], E. Heijne[j], S. Heising[c], S. Janos[g], L. Jungermann[e], I. Konorov[n], Z. Li[l], C. Lourenço[a], M. Mikuz[j], V. O'Shea[c], S. Pagano[h], V.G. Palmieri[a], S. Paul[n], S. Pirollo[f], K. Pretzl[g], P.Rato Mendes[b], G. Ruggiero[1,c], K. Smith[c], P. Sonderegger[a], P. Sousa[b], E. Verbitskaya[m], S. Watts[k], M. Zavrtanik[j]

[a] *CERN, CH-1211 Geneva, Switzerland*
[b] *LIP, Av. E. Garcia, P-1000 Lisbon, Portugal*
[c] *Department of Physics and Astronomy, University of Glasgow, Glasgow G12 8QQ, UK*
[d] *Low Temperature Laboratory, Helsinki University of Technology, FI-02150 Espoo, Finland*
[e] *IEKP University of Karlsruhe, D-76128 Karlsruhe, Germany*
[f] *Dipartimento di Energetica, Universitá di Firenze, I-50139 Firenze, Italy*
[g] *LHEP, University of Bern, Sidlerstarsse 5, CH-3012 Bern, Switzerland*
[h] *Dipartimento di Fisica, Universitá "Federico II" and INFN, I-80125 Napoli, Italy*
[i] *Department de Radiologie, Universite de Geneve, CH–1211 Geneva, Switzerland*
[j] *Jozef Stefan Institute, Exp. Particle Physics Department, PO Box 3000, 1001 Ljubljana, Slovenia*
[k] *Brunel University, Uxbridge, Middlesex UB8 3PH, UK*
[l] *Brookhaven National Laboratory, Upton, NY 11973-5000, USA*
[m] *Ioffe PTI, Russian Academy of Sciences, St. Petersburg 194021, Russia*
[n] *Physik Department E18, Technische Universität München, D-85748 Garching, Germany*

RD39 Collaboration

Abstract

We shall review test results which show that silicon detectors can withstand at 130 K temperature a fluence of $2 \times 10^{15}\,\mathrm{cm}^{-2}$ of 1 MeV neutrons, which is about 10 times higher than the fluence tolerated by the best detectors operated close to room temperature. The tests were carried out on simple pad devices and on microstrip detectors of different types. The devices were irradiated at room temperature using reactor neutrons, and in situ at low temperatures using high-energy protons and lead ions. No substantial difference was observed between samples irradiated at low temperature and those irradiated at room temperature, after beneficial annealing. The design of low-mass modules for low-temperature trackers is discussed briefly, together with the cooling circuits for small and large systems.

*Corresponding author. Tel.: +41-227676079; fax: +41-227678350.
E-mail address: tapio.niinikoski@cern.ch (T.O. Niinikoski).
[1] Also at CERN, Geneva, Switzerland.

0168-9002/02/$ - see front matter
PII: S0168-9002(01)01644-8

1. Introduction

Cryogenic semiconductor detectors have been used already for a long time, mainly in high-resolution nuclear spectroscopy. Typical examples are massive Ge detectors used in γ-spectroscopy, and Li-drifted Si detectors in X-ray spectroscopy. Our earliest experience dates back to 1974 when building a beam trigger detector sitting at 1 K temperature right in front of the cell of a frozen-spin polarized target [1] , the target itself running at 30 mK temperature. The detector, mounted in an evacuated box, consisted of two silicon surface barrier diode sensors, each 1500 μm thick, biased and read out via two 50 Ω coaxial lines which were connected to wide-band RF amplifiers. We observed but did not understand the detector polarization phenomenon, and could overcome it by reversing the 300 V bias potential for a few seconds every 24 h. This restored the electric field distribution and therefore the signal height. Cooling narrowed the current signals from 50 to 20 ns, and their height increased with roughly inverse ratio; this was a direct observation of the increased mobility. Moreover, the leakage current could be used for monitoring the evolution of the detector polarization, and it returned each time to zero after the bias was briefly reversed.

We feared that the growth of the leakage current and reduction of the signal would be due to radiation damage at the fluence of $10^{11}\,\mathrm{cm}^{-2}$ of 6 GeV pions. As no noticeable damage was known at room temperature and at these fluences, we thought that radiochemistry might work against us at these very low temperatures. We therefore failed to discover the detector polarization and other phenomena which are now known to be very important in applications requiring radiation hardness.

The detector polarization was predicted for Ge detectors already in 1974 [2], and it was later observed in silicon detectors in 1995 [3] . It was only very recently that the importance of polarization at cryogenic temperatures was fully understood, in view of applications requiring extreme radiation hardness. This followed the first observation in 1998 [4] of the Lazarus effect and the further studies of the RD39 Collaboration at CERN. The Lazarus effect is phenomenologically described as the recovery of the Charge Collection Efficiency (CCE) of heavily irradiated silicon detectors when cooled to cryogenic temperatures. Some results of RD39 were published on the studies of the CCE [5] , extending up to fluences about one order of magnitude higher than the limit of survival for usual silicon detectors. Results on the CCE and track resolution for a proton irradiated double-sided microstrip detector were also published already [6] .

In the present paper we shall review the highlights of our published experimental work carried out during the period of October 1998 until now. The design and construction of two simple cooling systems are described. We also include here some preliminary results on p^+np^+ diodes, on segmented devices, and on in situ irradiated devices. The annealing effects were investigated on some devices and are summarized here. Moreover, the design and construction of a prototype ''Beamscope'' tracker is described and preliminary test results are discussed.

2. Samples and experimental techniques

Prototype Si detectors were processed at Brookhaven National Laboratory (BNL), on 4″ float-zone wafers of different thicknesses and resistivities, using a process with three mask steps. The processed structures have a single guard-ring and the devices include several types of segmentation: single-pad and multipad diodes, and microstrip detectors with various pitches and strip widths. The p^+nn^+ or p^+np^+ pad and strip detector structures are described below.

A 0.47 μm SiO_2 layer was thermally grown on the n-type Si wafers. The first mask was used to open up windows (with 0.1 μm SiO_2 remaining) on the front side which define the detector geometry and allow B ion implant to go through and form the p^+ layer. During etching of the SiO_2 windows the back SiO_2 was etched uniformly; this allows a uniform implantation of P and B ions for the n^+ and p^+ layers, respectively. After implantation and thermal activation anneal in N_2, a second mask was used to cut the remaining 0.1 μm SiO_2

down to bare Si on the front side, while the SiO_2 layer on the back side was cut entirely. Al layers of 0.25 μm thickness were then sputtered on both sides. The third mask was then used to define the metal contacts on the front side. After a final thermal sintering in the forming gas (N_2 with 4% H_2), the detectors were ready for testing. This is the process with which the detectors discussed here were produced, with the exception of the sensors of the DELPHI module.

Irradiations of diodes with neutrons were performed at the TRIGA reactor of the Jozef Stefan Institute in Ljubljana, in the experimental channel positioned in the reactor core. The fluence for individual samples was determined by gold activation converted to NIEL with the measured spectrum and damage functions as described in Ref. [5] . The systematic error on the fluence measurement is about 10%. We shall report here results on sensors covering the equivalent 1 MeV neutron fluence range of 1×10^{14}–2×10^{15} n/cm^2.

A simple LN_2 cryostat devoted to CCE measurements was designed and built for laboratory tests at CERN and other institutes of RD39. The cryostat consists of an outer vacuum chamber of 100 mm diameter and an inner LN_2 reservoir. The top flange is equipped with access ports to the vacuum space where the sensor samples are mounted on PCB chip carriers. These ports carry the hermetic-seal feedthroughs for the detector and instrumentation wires, a vacuum gauge, and the vacuum pumpout valve.

Small interchangeable PCB chip carriers are mounted on a larger PCB motherboard which is connected to the LN_2 reservoir via a thermal bridge. The input FET of the preamplifier is located on the chip carrier. To improve the thermal conduction between the PCBs, their top plastic layers were partially removed so that the underlying gold-plated copper layers could directly touch each other.

A temperature of 78 K was reached on the detector mount with no applied heat load. A heater was positioned between the chip carriers of the detector under study and of the trigger detector. The maximum power of 1 W yielded the sensor temperature of 178 K.

The diode detectors were tested using a radioactive source and a charge amplifier with 1 μs shaping constant. Electrons passing through the diode were selected using a trigger detector placed behind, in order to choose near Minimum Ionizing Particles (MIPs). The CCE was determined by comparing the most probable value of the signal height of the irradiated detector with that of a similar but unirradiated detector, biased well above the full depletion voltage. If the spectrum could not be well fitted by a Landau distribution, the measurement was rejected. A typical spectrum obtained with a detector irradiated up to 1×10^{15} n/cm^2 is shown in Fig. 1.

Silicon pad detectors with p^+nn^+ structure were irradiated with 450 GeV protons of the SPS at 83 K temperature, in a continuous-flow liquid nitrogen cryostat equipped with thin windows. The detectors were biased during irradiation and signals were read out, at lower beam intensity, with a charge amplifier having a shaping constant of 2 μs placed just outside the cryostat. Preliminary results are reported in Section 5.

In these in situ measurements of the radiation damage two beam configurations were used. During the irradiation phase the high intensity

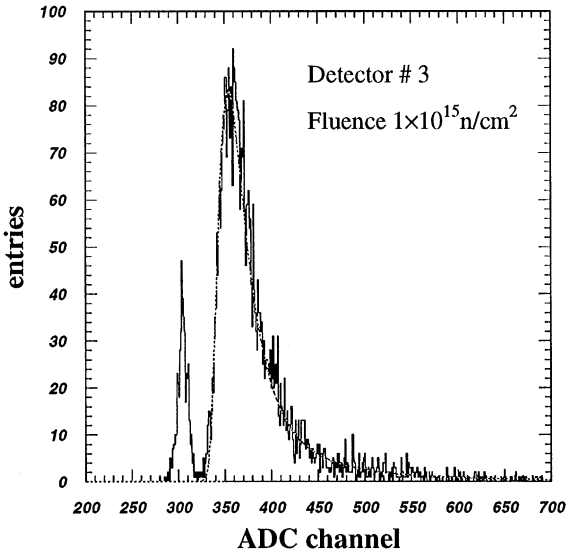

Fig. 1. A typical charge distribution obtained from a detector irradiated up to a fluence of 1×15 n/cm^2, operated at 77 K under 250 V reverse bias.

proton beam of the NA50 experiment was focused on one of the pads of the detector using a wire chamber just before the cryostat. The pad was then irradiated at maximum intensity (few 10^{10} p/burst) for some hours until 2×10^{12} protons were accumulated. This corresponds to an equivalent dose step of about 10^{14} p/cm^2 at the pad, given at a dose rate of about 1 Mrad/h. The beam intensity was then lowered to 10^5 p/burst at 300 GeV by inserting an aluminium target 118 m upstream of the detector, thus generating a wide secondary beam used for the measurement of the CCE. These two steps were repeated until the maximum fluence of about 1.2×10^{15} p/cm^2 was reached. This would correspond to a 1 MeV neutron fluence of about 6×10^{14} n/cm^2 [9], but is based only on extrapolation of existing data, since no damage conversion factors for particles of such high energy are available.

Pad detectors were also irradiated in the continuous-flow cryostat at 80 K temperature in the 158 GeV/nucleon high-intensity lead ion beam of the CERN SPS. The beam was steered and focused onto one of the pads of the detector. The beam intensity could be adjusted between 10^5 and 10^9 ions/burst; the burst duration was 5 s and interval 12 s.

We also tested, in collaboration with the COMPASS and LHCb experiments, a rejected half module of the 1994 DELPHI vertex detector [5]. The results were described in detail in Ref. [6] . The module consists of two AC-coupled double-sided silicon microstrip sensors with a sensitive area of 3.2×5.4 cm^2, daisy chained together and bonded to a double-sided hybrid. The p^+-sides of the detectors have strips with a pitch of 25 μm, with every second strip being read out. The n^+-sides of the detectors have strips with a pitch of 42 μm which run perpendicular to the p^+-side strips; the n^+-side strips are separated by p^+ blocking implants. The n^+-side signals are routed to the same short side of the detector plate where all bonding pads are located, using a second metal layer. The total number of strips in the module is 1280. The hybrid is equipped with ten MX6 CMOS analog readout ASICs with a shaping constant of 8 μs; these circuits are not radiation tolerant.

The DELPHI microvertex detector half-module was irradiated at room temperature with 24 GeV protons at the CERN PS, in collaboration with the LHCb experiment. During irradiation the detector was not biased. The fluence was determined from the activation of aluminium. The fluence was non-uniform and reached a maximum of 3.5×10^{14} p/cm^2 corresponding to an equivalent fluence of 1.9×10^{14} n/cm^2. This detector drew a total current of 1 mA at 65 V at room temperature after irradiation, and it was operated at cryogenic temperatures in the SPS test beam as described in Section 6.

A strip detector with 50 μm pitch was designed as a sensor for a beam hodoscope (Beamscope) tracker prototype module where two perpendicularly positioned sensors provide one x–y point. The Beamscope will be discussed in Section 7. The detector has p^+nn^+ structure described above. The p^+-side has 24 strips of 5.135 mm length with 50 μm pitch and 15 μm width in the central region, 4 large strips of the same length with 500 μm pitch and 450 μm width on each side of the central region, and one active guard ring. The simple DC coupled design required only two masks thus reducing significantly the processing cost of the sensor.

The Beamscope detector modules, shown in Fig. 2, were built by gluing glass-epoxy Printed Circuit Boards (PCB) through slots machined on stainless steel flanges with a filled epoxy. The epoxy is resistant to thermal shocks at low temperatures and has a high thermal conductivity. The PCB has five copper layers which were designed so that the thermal conduction between

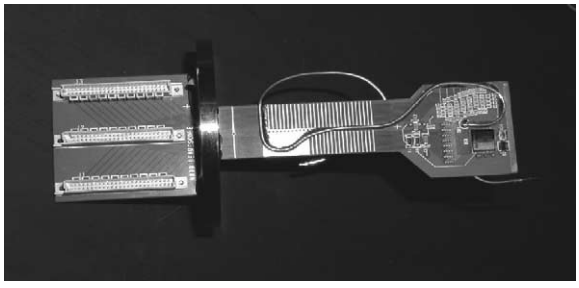

Fig. 2. The Beamscope PCB containing two detectors mounted back-to-back and rotated 90°.

the flange and the sensors was low, whereas the transverse conduction was improved by the patterning of the ground layers.

A thin-wall capillary pipe of 1.2 mm outer diameter, made of cupronickel, is soldered along the PCB (Fig. 2). The pipe is fed from the transfer line and its outlet is connected to a flow meter and a manual control valve.

A continuous-flow LN_2 cooling system was designed for operating these detector modules at temperatures between 80 and 185 K. This system consists of a top flange equipped with five access ports for five modules, ports for a LN_2 transfer line and a cryogenic needle valve, and additional ports for instrumentation connections. The flange can be optionally placed onto a vacuum chamber or on a foam-isolated chamber filled by N_2 gas. In the foam-isolated chamber with inner dimensions of $94 \times 140 \times 370$ mm, operation at 80 K is possible by two-phase flow of nitrogen through capillary pipes integrated in the modules, while higher temperature operation requires the flow of gas only in the modules.

In the vacuum chamber the cryogenic needle valve can, in principle, be used for controlling the coolant flow through a thermal radiation shield, but it was found that this was not necessary when some superisolation was applied around the modules. The control of the module temperature up to 185 K was possible by adjusting the flow through the modules and the power applied by heaters on the modules.

The prototype Beamscope tracker was exposed to the 40 GeV/nucleon lead ion beam of the SPS. During this run the microstrip detectors described above received a total dose of about 1 GRad and showed no sign of deterioration of the signal.

3. Experimental studies of the Lazarus effect in p^+nn^+ diodes

The DC-coupled p^+nn^+ implanted silicon diodes, irradiated by neutrons at room temperature as discussed above with fluences of 1×10^{14}, 5×10^{14}, 1×10^{15} and 2×10^{15} n/cm^2, have a sensitive area of 5×5 mm^2 and various thicknesses.

The temperature dependence of the CCE, determined using a β-source as described above, was recorded during a slow cooldown and is shown in Fig. 3. The CCE starts to rise below 180 K and reaches a maximum at about 130 K for all samples. The slight decrease of the CCE observed below 130 K also has a universal character. The heavily irradiated detectors do not reach 100% CCE at the maximum applied bias voltage of 250 V. The temperature scan of the less irradiated detector was also performed at 250 V which is high enough to fully deplete the device even at intermediate temperatures. The CCE is then close to 100% at all temperatures at which the noise level allowed to perform measurements, suggesting that the non-linear increase in CCE at low temperature (know as the Lazarus effect) is due to a combination of the increased depletion depth and of the temperature dependence of trapping.

In materials rich in deep-level traps (such as silicon after heavy irradiation), the history of the bias voltage plays a crucial role in the time evolution of the amplitude of the signal at cryogenic temperatures. For example, reversing

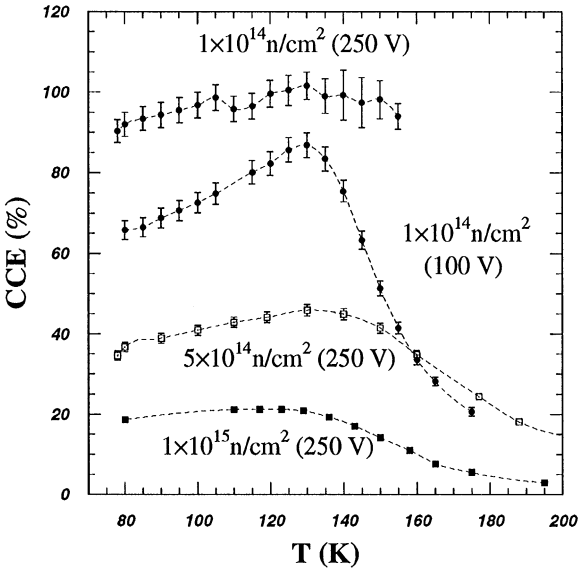

Fig. 3. Temperature dependence of CCE for three detectors irradiated with neutron fluences of 1×10^{14}, 5×10^{14}, and 1×10^{15} n/cm^2, in reverse bias.

the bias polarity generates a transient condition in the bulk, during which the radiation-induced electrical pulses are gradually reduced in amplitude, and change sign only after a few minutes. This process was originally observed in germanium detectors [2] and was called "detector polarization". Measurements repeated after turn-on of the reverse bias voltage yield a monotonically decreasing CCE converging towards a stable reduced value. In the p^+nn^+ diodes the decrease took place in the first 30 min after which the CCE remained stable. Most of the CCE loss takes place in the first five minutes after the HV is applied. It is also important to note that in the detector irradiated up to 10^{14} n/cm^2 it is possible to completely suppress the time dependence of the CCE by means of a fairly large bias voltage which corresponds to a strong overdepletion. A confirmation that this situation is stable comes from the data of Fig. 3, where the CCE measured at 250 V stays constant at 100% during the temperature scan.

There is no physical reason for the time dependence of the CCE to be exponential, because the mechanism is based on the time evolution of the electric field distribution in the bulk [7] . Depending on the applied voltage, the detector may stay fully depleted for some time during which the CCE is close to 100%. At low temperatures the space charge and therefore the electric field will evolve so that the field may reach zero at the p^+ implant only after a delay time, after which the CCE will begin to decrease in a complicated way which may depend also on the charge integration time of the amplifier.

The voltage dependence of the CCE for the detector irradiated up to 10^{15} n/cm^2 was measured at 77 K. The maximum CCE obtained immediately after applying the HV, shows a increase with the voltage up to around 70% at 200 V. However, measurements taken at a given non-zero time after the HV is turned on yield a smaller value of CCE. The stable CCE values match the poor results obtained for the CCE in the temperature scans. Similar results have been obtained with other detectors irradiated with different fluences, with the exception of the maximum value reached. While the diode irradiated to 10^{14} n/cm^2 appears to be fully depleted at 250 V, those with higher fluence seem to require a higher voltage for full depletion which was not possible in the setup used in these measurements.

In a second set of experiments the detector was illuminated by light sources of various wavelengths in order to enhance the steady state current by means of optically generated non-equilibrium carriers. This was done in order to fill the radiation induced traps and to achieve a better penetration of the electric field in the bulk material of the detector. The intensity of the applied light was adjusted so that the leakage current was about 5 nA, not adding a significant contribution to the overall noise of our measurement system. The main effect of the light illumination is that no time dependence of CCE is observed. Under reverse bias operation, illuminating with short wavelength light (yellow or green), results in the stabilization of the good values of CCE normally obtained immediately after switching on the HV, but without temporal decay.

Forward bias operation has been considered very interesting for heavily irradiated silicon detectors, and promising results have already been obtained in the case of moderate cooling [8] . At lower temperatures one cannot distinguish this mode from the conventional reverse bias operation by judging from the current passing through the detector, due to very high bulk resistivity of the heavily irradiated silicon. Moreover, under these conditions the time dependence of the CCE is suppressed.

The temperature dependence of the CCE under forward bias is shown in Fig. 4. The CCE starts increasing around 180 K and saturates below 130 K, for all detectors. The measured values are about three times higher than those observed under reverse bias. Moreover, good values of CCE are recorded as soon as the noise induced by the bias current is low enough to allow measurement. The observation of good CCE values for these relatively high temperatures is in good agreement with previous observations [8] . However, the large leakage current near room temperature limits the application to finely segmented devices.

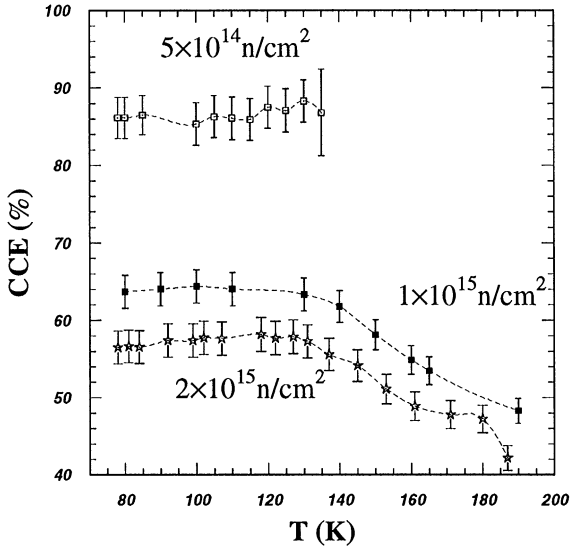

Fig. 4. Temperature dependence of the CCE for detectors irradiated with different neutron fluences, operated at 250 V forward bias. Note that the zero of the vertical axis is offset in this plot.

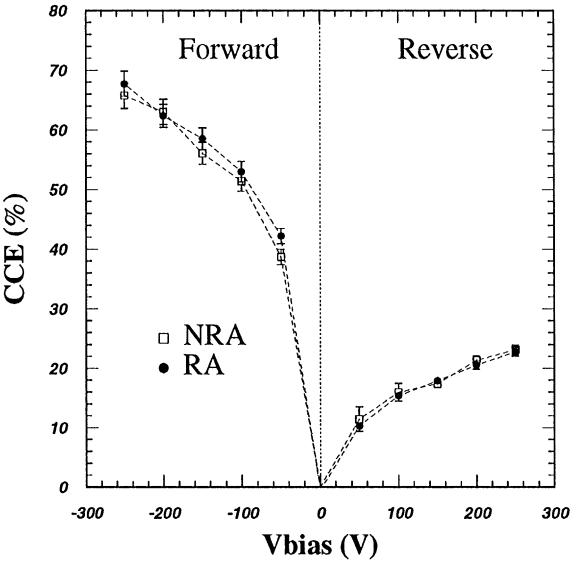

Fig. 5. Effect of reverse annealing on the voltage dependence of the CCE for detector irradiated up to 10^{15} n/cm^2. The measurements cover the full-allowed voltage range including forward bias. At reverse bias only stable CCE values are plotted.

The voltage dependence of the CCE under reverse and forward bias was measured at 77 K. The CCE is about three times higher with forward bias than with reverse bias in stable conditions. These large values are the same of those observed under reverse bias immediately after switching on the HV. The measurements could be extended to ± 250 V only because of the design of the apparatus, and the data suggests that the CCE continues to grow beyond the ultimate voltages, in particular for the reverse bias condition. This is an indication that the detector is only partially depleted due to its polarization.

The possible effects of the reverse annealing on the CCE recovery were investigated on a sample irradiated up to 1×10^{15} n/cm^2. The CCE was measured before and after a room temperature annealing period of about 1 year over the full allowed bias range, as shown in Fig. 5. No significant difference is found between these two sets of measurements. This suggests that the deep defects, which can be deactivated at low temperatures, are formed during (or soon after) irradiation at room temperature, and are not seriously affected by the reverse annealing.

4. Study of the symmetric p^+np^+ structures

After irradiation which inverts the bulk type, the conventional p^+nn^+ structure changes to p^+pn^+ and continues to behave like a diode, except that the junction develops from the n^+ implant instead of p^+. At low temperatures and under reverse bias, the CCE of such a diode degrades with time until it reaches a stable reduced value, but operation under forward bias is possible and yields a high and time-independent CCE, as was discussed above. To avoid the detector polarization and time dependence of the CCE, one could therefore use a standard diode detector under reverse bias until the resistivity of the type-inverted bulk, increasing with the accumulated dose, is large enough to enable operation under forward bias. This has the impractical drawback that bipolar electronics must be used to read out the detector signal and to supply the high-voltage bias. Alternatively the reverse bias current can be controlled by illumination with visible light so that the electric field is flat, thus preserving the

initial high value of the CCE. However, this technique might prove unfeasible for large trackers.

In a more practical approach one can consider devices designed to take full advantage of cryogenic temperatures. We have investigated in particular a symmetric p^+np^+ implanted silicon detector which can be viewed as a series of two diodes connected in opposite directions. Below the breakdown voltage the detector conducts at neither polarity of the bias voltage, because one of the diodes is under reverse bias in each case. After type inversion, it is expected that the detector does not have the double-diode characteristic any more, but behaves as high-resistivity silicon with ohmic contacts. According to this scenario, one would expect the detector to have the following properties: the CCE is symmetric under forward and reverse bias, and after type inversion there is no decay of the CCE with time.

The investigated p^+np^+ sample is one of those discussed in Section 2. It has a sensitive area of $5 \times 5\,mm^2$, thickness of 400 μm, and was irradiated with neutrons at room temperature up to a fluence of $1 \times 10^{15}\,n/cm^2$ which largely exceeds the bulk type inversion threshold. The results discussed below are based on our preliminary analysis.

The *I–V* characteristics of the investigated sample features a symmetric behaviour at room temperature. The current is $\sim 0.2\,mA$ at a voltage of 10 V and is of the same order of magnitude as the current measured for a standard p^+nn^+ silicon detector under forward bias irradiated to a comparable dose. The bias current at 77 K is less than 1 nA up to 500 V.

The CCE was measured at three different temperatures; the preliminary results are shown in Fig. 6 as a function of the applied bias voltage. The values shown in the figure correspond to the stable values of the CCE (30 min after voltage turn-on).

The plot clearly shows the expected symmetry of the sample for positive and negative applied bias voltage. The CCE increases with the absolute value of the applied voltage and a maximum CCE of $84 \pm 4\%$ is achieved at 500 V and $T = 130\,K$ in agreement with previous experimental observations. Above 200 K and bias voltages beyond

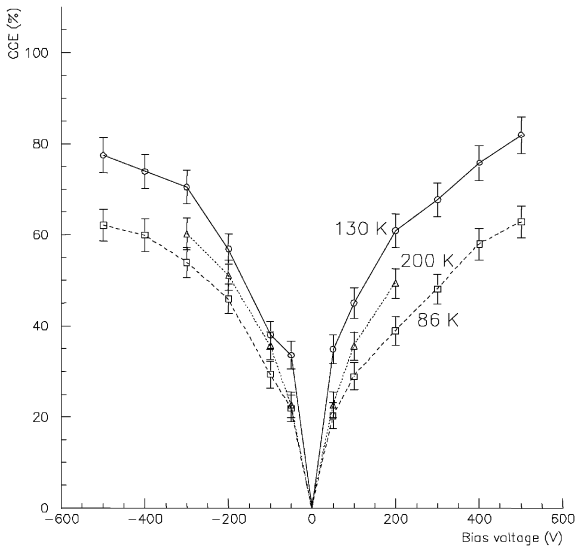

Fig. 6. The CCE of the irradiated p^+np^+ sample versus bias voltage at different temperatures. All measurements are taken 30 min after bias voltage turn-on. The fluence was $1 \times 10^{15}\,n/cm^2$.

$+200\,V$ or $-300\,V$ the large leakage current affected the measurement so that it was impossible to fit the data with a Landau distribution.

The time evolution of the CCE at 86 K was measured at several positive and negative bias voltages. The device does not have a completely ohmic behaviour, but it rather "remembers" that it is made of semiconductor material with deep trapping levels. At 500 V the CCE decays $8 \pm 1\%$, while at 50 V the decay is $13 \pm 1\%$: the time dependence clearly decreases with increasing bias voltage.

In Fig. 7 the evolution of CCE is shown at 500 V bias and at several temperatures. One can conclude that the decay of CCE becomes smaller at higher temperatures: at 200 K there is little time dependence.

In summary, at a given temperature the CCE shows a decay with time which is smaller for larger bias voltages and at higher temperatures. The time dependence turns out to be much smaller than that a standard detector in reverse bias. For comparison, the CCE of the standard detector at 200 V decays from an initial value of $\sim 70\%$ to $\sim 20\%$ in 30 min at a temperature of about 80 K. At the

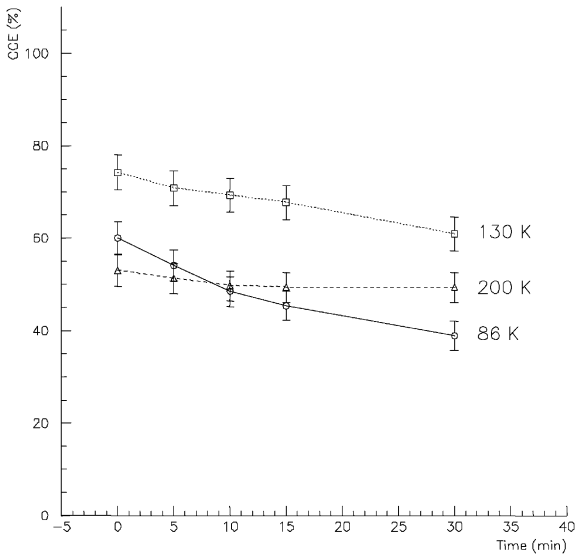

Fig. 7. The CCE of the irradiated p^+np^+ sample versus time after voltage turn-on. The measurements were taken at a bias voltage of 500 V for three different temperatures.

same temperature and bias voltage, and in the same period of time, the CCE of the p^+np^+ detector decays from ~60% to ~40%. At 500 V the CCE of the symmetric detector does not decrease below 60%.

The CCE measurements of the symmetric detector were made with the preamplifier shaping time constants of 1 μs and 0.25 μs, in order to investigate any influence of the charge transit time on the collected charge. Both shaping times give the same value for the CCE at 130 K within the error bars. Measurements under other circumstances (i.e. different temperatures and time intervals after voltage turn-on) give similar results and verify that the charge transit time is fast enough for the signal to be amplified with a shaping time of 250 ns.

5. Diode detectors irradiated in situ at cryogenic temperatures

The above studies have proved that at low temperatures silicon detectors tolerate radiation damage which is accumulated at room temperature. However, no previous investigations have been made on the radiation hardness of detectors irradiated in situ at low temperatures. We therefore studied DC-coupled p^+nn^+ implanted silicon pad detectors processed and irradiated as discussed in Section 2, using the SPS proton beam. The sensitive area of the pads was $1.2 \times 1.2\,mm^2$, and the thickness of the sensor was 400 μm.

As was described in Section 2, the pad detector was irradiated in steps to the fluence of about $1.2 \times 10^{15}\,p/cm^2$ in the 450 GeV proton beam at the CERN SPS, equivalent approximately to a 1 MeV neutron fluence of about $6 \times 10^{14}\,n/cm^2$ [9] based on extrapolation of existing data.

The current-voltage characteristics for the irradiated pad under reverse bias was measured while biasing the guard-ring at the voltage of the pad, in order to measure the bulk current only. The maximum applied voltage was 500 V. The *I–V* characteristic was measured at 300 K for the irradiated pad. The leakage current is dominated by the generation component and is proportional to the square root of the bias voltage. At 83 K the leakage current is less than 1 nA up to 500 V.

The measured CCE was normalised to that before the irradiation, which reaches 100% CCE at 50 V. Each measurement was performed after the detector had been left unbiased for a few minutes to allow depolarisation. Then, after having biased the detector, the time evolution of the CCE was monitored.

The CCE increased with the reverse bias voltage. Starting from 100% CCE at 100 V for zero dose, the stable CCE was seen to decrease to 80% at $3 \times 10^{13}\,p/cm^2$ and to 50% at the fluence of $1.2 \times 10^{15}\,p/cm^2$. At this dose, increasing the bias voltage up to 200 V results in a maximum CCE of 65%. The CCE varies almost linearly with voltage in this range, suggesting a higher value of the CCE for even higher bias.

It is interesting to note that the time evolution of the CCE at the maximum fluence $1.2 \times 10^{15}\,p/cm^2$ is small before annealing for 1 h at 200 K and increases after cooling back to 83 K. The beneficial annealing cannot be easily characterised when irradiating at room temperature since it takes place continuously during the irradiation process.

This may not be the case when irradiating at cryogenic temperatures if the activation energy is higher than $k_B T$. At the maximum fluence, after the beneficial annealing took place, a recovery of CCE up to 80% at 50 V bias was observed at 83 K temperature. A further increase of the bias voltage to 200 V results in a CCE value of 95%. The increase in CCE due to beneficial annealing is supposed to quickly disappear when the detectors are held for a long time at room temperature (reverse annealed), and measurements to verify this are currently in progress.

A more complete account of the in situ irradiation test can be found in these proceedings [9] .

6. CCE and resolution of the DELPHI detector under reverse bias

A measurement of the cluster shape both on the ohmic (n^+) and on the junction (p^+) sides of the double-sided detector yields an estimate for the depth of the depleted layer. Using also the relationship between the depletion depth and the CCE, the integrated charges in the clusters of the junction side provides an independent estimate for the depth.

The DELPHI detector module which was described briefly in Section 2, was irradiated in the CERN PS. The beam profile was made inhomogeneous in order that the front-end read-out ASICs would not get damaged. The CCE of the damaged regions of the detector enabled to check the dose distribution which was measured using an aluminium activation foil. The maximum fluence was 3.5×10^{14} p/cm^2 on a 1 cm^2 spot in the central part of the detector.

The test of the irradiated detector was performed in the COMPASS 100 GeV/c muon beam of the CERN SPS. Tracks were reconstructed using a telescope consisting of three stations of silicon microstrip detectors allowing an unambiguous de-convolution of the resolution of the individual detectors. The irradiated module was placed in a cryostat together with a similar non-irradiated reference module and was kept at temperatures ranging from 115 to 140 K. As in the diode detectors, the CCE increased with the applied voltage and degraded with time, and the history of the bias voltage played a crucial role.

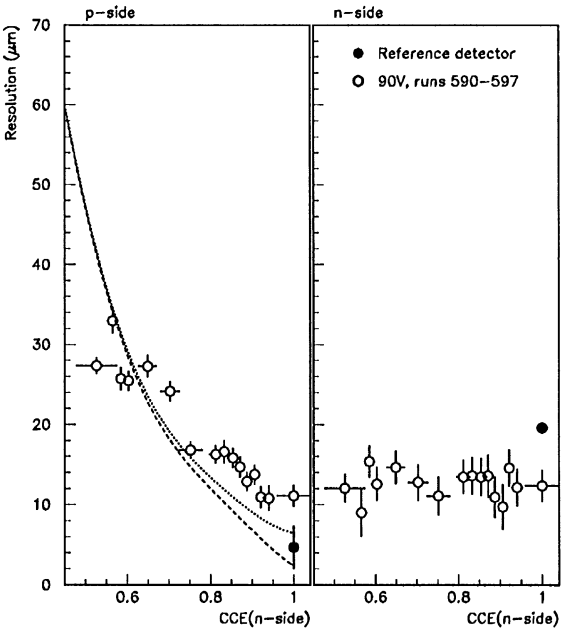

Fig. 8. Resolution for the p^+-side and the n^+-side, as a function of CCE (n^+-side). Note that the reference detector has a n^+-side pitch double that of the irradiated detector. The dotted curves show a Monte Carlo simulation.

The experimental and simulation results are summarized in Fig. 8. The resolution on the p^+-side of the reference detector was found to be around 5 μm, in agreement with the expectation for 25 μm pitch with every second strip read out. The resolution on the n^+-side of the reference detector was found to be 19 μm, as expected for 84 μm strip pitch and perpendicular tracks. The resolution on the n^+-side of the irradiated detector, at the most damaged spot, shows no dependence on the CCE. Since the S/N for full depletion was measured to be around 18, and the detector depletes from the n^+-side, this was expected. The measured value is around 12 μm, whereas one would expect around 9 μm for a detector with 42 μm strip pitch. The resolution on the p^+-side of the irradiated detector is 12 μm in the case of full depletion and worsens rapidly with

decreasing CCE. The dotted curves show two Monte Carlo simulations for the resolution, made with a method described in Ref. [6] .

7. A prototype beam hodoscope for heavy ions

The prototype beam hodoscope (Beamscope) for fixed target heavy ion experiments such as NA60[2] is the first application of radiation hardened silicon detectors based on the Lazarus effect. The experiment requires the recording of individual lead ion tracks with the position resolution of 10 μm upon delayed trigger signal from another subdetector. The Beamscope should work in the beam of around 10^7 ions/s, and the total accumulated dose at the beam spot on the sensors will reach 100 GRad.

Based on the above encouraging results on silicon microstrip sensors, a detector with 50 μm pitch was chosen for the Beamscope prototype. The sensor design features narrow central strips and wide strips on each side, and was described in Section 2. The wide strips were connected to current-to-frequency converters located outside the cryostat. The frequencies produced by these converters were proportional to the rate of the lead ions traversing the strips, and were recorded by CAMAC scalers. This information was used for coarse beam steering and was found to be very efficient. Online monitoring based on narrow-strip scaler data was used for accurate beam steering.

The detectors were mounted on a PCB of Fig. 2 and were placed in the vacuum chamber of the continuous-flow cryostat; these were discussed in Section 2.

The narrow detector strips and the backplanes were connected via 100 Ω microstrip transmission lines on the PCB to fast amplifiers, located on four printed boards outside the cryostat. The lines were terminated on both ends with matched loads. AC-coupling was used for the backplane signals. The amplified signals were connected to discriminators with programmable threshold, and the amplified backplane signals were also sent to a digital oscilloscope.

The discriminator signals of the narrow strips were used for tracking, and were also counted by means of CAMAC scalers. For the tracking, the signals during the last 3.4 μs were stored in a multi-hit time recorder system (MHTR), which covered well the latency of the forward calorimeter trigger of NA50, used for this test. The MHTR system, consisting of 12 CAMAC modules, was designed and built specially for this experiment, and did not require any computer intervention during the beam spill, since the data were transferred and buffered in a CAMAC memory module which was read out after the spill.

The operation of the MHTR is based on interleaved digital sampling technique which increases the effective sampling rate to 600 Ms/s. The sampled signal of each microstrip is stored in a circular buffer for 3.4 μs. The arrival time of the trigger signal is determined with same interleaved sampling technique. The contents of the circular buffers are frozen at the arrival of a trigger signal. The data-reduction and read-out logic then encodes the selected strip data together with the channel number in an appropriate way, and writes the data to the buffer memory module. Strong data reduction can be achieved, especially for high beam intensity, by accepting only hits in a time window corresponding to the trigger delay.

The backplane signal was 200 mV for 200 V bias voltage and has been acquired directly by a digital oscilloscope at 8 GS/s. A signal at 50 V bias voltage is shown in Fig. 9, illustrating the rise time of $\leqslant 0.5$ ns and the 20 ns tail of the signal. The rise time is that of the oscilloscope. Shapers were introduced to reduce the 20 ns tail. The coincidence of the backplane signals can be used for triggering the detector readout. The timing characteristics of these signals are better than those of scintillators, and a faster amplifier can be used.

The distribution of the delay between the strip and trigger signals has a width of a few ns which leads to an efficient selection of the beam particle whose interaction caused the trigger.

During this test beam period the detectors received a maximum dose of about 1 GRad and showed no sign of deterioration of the signal. With

[2] Proposal CERN/SPSC 2000-010, SPSC/P316, 7 March 2000.

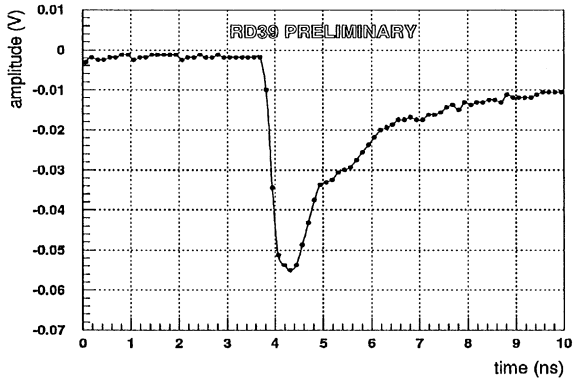

Fig. 9. Unshaped current signal of the Beamscope detector backplane.

the possibility to increase voltage by a factor of 10 and because a 10 times smaller signal is still readable, we are confident that the system can be operational up to much higher doses.

8. Design of low-mass detector modules and large trackers

The choice of materials for the construction of low-mass detector modules is guided by their thermal and mechanical properties, in addition to the radiation length. The thermal path from the sensors and readout electronics to the coolant must be highly conductive, while it is desirable that the sensors are thermally isolated from the readout electronics. The materials joined together must have similar thermal dilatation unless the thermal stress can be relieved by the geometric shape of the structures. The materials with low conductivity must be resistant to the stress due to a thermal shock.

The above requirements are equally important to the detectors operating at $-15^{\circ}\mathrm{C}$ ($=258\,\mathrm{K}$) and to those running at 130 K, and the design principles of the cryogenic low-mass modules are therefore very similar to those used for the LHC experiments. We shall therefore abbreviate our discussion and mainly focus on the main differences in the materials at these temperatures.

The thermal conductivity of good conductors increases at low temperatures, while that of good thermal isolators decreases. These make the thermal design easier at low temperatures. Examples of good conductors are silicon, pure metals (Cu, Al), and thermal pyrolytic graphite (TPG). Some poor conductors used in the modules are fused quartz and other glasses, epoxies and composites such as carbon fibre composite (CFC) and glass-epoxy. Metal alloys are also relatively poor conductors. Intermediate cases are ceramics such as BeO, Al_2O_3 and AlN whose conductivity is fairly good but is somewhat reduced at low temperatures.

The reverse current at constant voltage in irradiated diodes follows the law

$$\frac{I}{I_0} = \left(\frac{T}{T_0}\right)^n \exp\left[-\frac{E_j}{k_B}\left(\frac{1}{T} - \frac{1}{T_0}\right)\right] \quad (1)$$

where I_0 is the current at a fixed (e.g. room) temperature T_0, $E_g = 0.63\,\mathrm{eV} \approx E_g/2$ is the effective current-activation energy, and n has been found to fit well the value of 2 if E_j is assumed constant. The current is therefore strongly suppressed by reducing the temperature, and the heat dissipation is so small that the thermal conductivity of the silicon sensor is sufficient for providing good thermal uniformity and stability against thermal run-away.

The best thermal dilatation match with silicon is obtained by using silicon also as a structural material. Electrical isolation is obtained by coating the silicon with thermally grown SiO_2. The baseboard of the hybrid readout circuitry can be thus made of silicon which provides a high conductivity and excellent match of dilatation with the readout ASICs. Silicon can also be used as spacers between sensors mounted back-to-back in a module.

The thermal dilatation of filled epoxies and composites can be approximately matched with that of silicon or other materials. Suitable fillers are quartz and chalk powders. The CFC can be matched by the choice of the fibres and their density ratio. TPG as a hybrid baseboard can be matched to the silicon of the ASICs by sandwitching it between thin layers of other material with strong dilatation.

The design of an end-tapped microstrip detector module with back-to-back sensors can be simplified greatly when using a suitable 2-phase coolant at a high pressure, because then the cooling pipe can be so small that it can be integrated in the module structure between the sensors and the hybrid, sandwitched under the fan-ins. With 12 APV25 chips in a module with 1536 strips the total thermal losses are about 3.5 W which requires the mass flow of 2-phase Ar of less than 4 mMol/s. If the coolant temperature is 110 K, the pressure drop limits the inner diameter of the pipe to 0.3 mm. Such a pipe can be easily integrated inside the module structure.

The low-temperature detectors are most comfortably operated under high vacuum which has the inconvenience that relatively thick walls must be used to avoid elastic instability. The vacuum must be good enough so as to avoid discharge in the residual gas and contamination of the cold detector surfaces by condensible vapours. Operation in pressurized nitrogen or argon is also possible but has the inconvenience that convection will cause a substantial heat load on the sensors, requiring a more massive design of the modules.

As vacuum is already available inside the beam pipe and in the cryostat of the superconducting solenoid of a modern tracker, it becomes tempting to design future trackers so that there is no pressurized volume between the beam and the solenoid. The beam pipe can then be made very thin because it does not need to support a differential pressure.

Long-term operation in an environment with high radiation field and limited access requires a cryogenic coolant storage and distribution system, or a closed-cycle refrigeration system. An additional point of concern is the safety risks of liquid nitrogen which may become explosive at fluences already below 10^{17} p/cm^2. The limited access precludes the use of transport dewars and forces to install long transfer lines between the cryostat and the storage tanks located in an accessible area.

Among the closed-cycle coolers the Stirling cycle engines and Gifford–McMahon cryogenerators are presently the most efficient and are suitable for small trackers with up to 10^5 readout channels. The cooler must be supplemented by two-phase coolant distribution which consists of a condenser and a cold liquid pump, or of a J-T cycle involving a heat exchanger, condenser, expansion orifice, and a warm compressor which can be located outside the radiation environment.

The suitable coolants around 130 K temperature are perfluoromethane CF_4, Kr, methane CH_4, and Ar. Their practical two-phase and J-T cycle temperature ranges are between their normal boiling points and critical points listed in Table 1. Nitrogen covers temperatures below this range but is impractical close to its critical point of 125.98 K. It should be noted that the same circuit design and compressor can be used with all of these fluids, and therefore the temperature of operation can be changed simply by evacuating and refilling the two-phase coolant distribution system. The cryogenerators use helium as working fluid.

In a large tracker with magnetic field the use of a cryogenerator and a liquid circulation pump would require a substantial development effort to replace the metallic moving parts with non-conducting structures, and the electrical motors with pneumatic drives. Vacuum-isolated cryogenic transfer lines provide a major space saving in such trackers, and the thermal losses of such lines are less than a few W/m. Cooling systems designed for absorbing the heat loads of more than 1 kW are therefore not dominated by the losses in the transfer and storage.

The structural stability of all materials is improved at low temperatures because creep becomes very slow, and even the softest glasses have their glass transition above 130 K. The thermal stresses, on the other hand, can become

Table 1
Normal boiling points and critical points of some coolants in the temperature range around 130 K

Coolant	Normal boiling point (K)	Critical point (K)
CF4	145.10	227.51
Kr	119.75	209.39
CH4	111.67	190.60
Ar	87.27	150.65

a problem unless taken into account in the design phase. The metrology of the structures cannot be made at low temperatures by mechanical means; therefore the coarse measurements at room temperature must be supplemented by optical methods which work in situ. The alignment methods of the cryogenic detector are similar to usual detectors and are based on the recording of straight tracks of charged particles, or on the use of a narrow X-ray beam.

9. Conclusions and implications for the collider experiments

The results of the RD39 Collaboration suggest that silicon detectors can withstand at low temperatures fluences of at least $2 \times 10^{15}\,\mathrm{n/cm^2}$ which is 10 time more than the limit of the most sophisticated LHC detectors. The detector design becomes simpler and entails substantial savings in the processing costs. Large standard wafers can be used and therefore 12 cm long modules can be built without daisy chaining. This also simplifies the assembly of modules.

The thermal design and cooling are easier at low temperatures than close to room temperature, because in the first case the sensor dissipation is almost zero and thermal conduction is favourable. The coolants are simple 2-phase fluids such as Ar which avoids any radiochemical and corrosion problems. The use of vacuum isolation forces to change the concept of access, but entails no major technical problem. A simple solution is to combine the magnet and tracker teams so that a coherent mechanical design and easy integration can be achieved.

The use of silicon detectors in already existing cryogenic systems is clearly prescribed. Examples of these are preshower detectors for Ar calorimeters, an beam loss monitors in superconducting beam steering and focusing magnets. Commercial applications of the cryogenic silicon detectors may be found in X-ray and hadron radiotherapy.

Acknowledgements

This work carried out by the RD39 Collaboration would not have been possible without the support of the CERN management and the NA50, COMPASS and LHCb experiments, and we are grateful to their participating members. The support of the ATLAS, CMS and TOTEM experiments is also greatly appreciated and acknowledged. We have furthermore profited from discussions with the CERN Beam Instrumentation group and would like to thank them for their helpful advice.

References

[1] T.O. Niinikoski, F. Udo, Nucl. Instr. and Meth. 134 (1976) 219.
[2] V.K. Eremin, N.B. Strokan, N.I. Tisnek, Sov. Phys. Semicond. 8 (1974) 751.
[3] V. Eremin, Z. Li, I. Ilyashenko, Nucl. Instr. and Meth. A 360 (1995) 458.
[4] V.G. Palmieri, K. Borer, S. Janos, C. Da Viá, L. Casagrande, Nucl. Instr. and Meth. A 413 (1998) 475.
[5] K. Borer, S. Janos, et al., Nucl. Instr. and Meth. A 440 (2000) 5.
[6] K. Borer, S. Janos, et al., Nucl. Instr. and Meth. A 440 (2000) 17.
[7] B. Dezillie, V. Eremin, Z. Li, E. Verbitskaya, Nucl. Instr. and Meth. A 452 (2000) 440.
[8] A. Chilingarov, T. Sloan, Nucl. Instr. and Meth. A 399 (1998) 35.
[9] G. Ruggiero, et al., Nucl. Instr. and Meth. A 476 (3) (2002), these proceedings.